Applied Materials Today 27 (2022) 101449

Contents lists available at ScienceDirect

Applied Materials Today

journal homepage: www.elsevier.com/locate/apmt

Self-winding liquid crystal elastomer fiber actuators with high degree of freedom and tunable actuation

Zhiming Hu[a,b,c], Yunlong Li[b,c], Tonghui Zhao[a,b,c], Jiu-an Lv[b,c,*]

[a] School of Materials Science and Engineering, Zhejiang University, Hangzhou, Zhejiang Province 310027, China
[b] Key Laboratory of 3D Micro/Nano Fabrication and Characterization of Zhejiang Province, School of Engineering, Westlake University, 18 Shilongshan Road, Hangzhou, Zhejiang Province 310024, China
[c] Institute of Advanced Technology, Westlake Institute for Advanced Study, 18 Shilongshan Road, Hangzhou, Zhejiang Province 310024, China

ARTICLE INFO

Article history:
Received 11 January 2022
Revised 1 March 2022
Accepted 13 March 2022

Keywords:
Fiber actuator
Liquid crystal elastomers
High degree of freedom
Self-winding

ABSTRACT

Liquid-crystal-elastomer (LCE) fiber actuators capable of reversible, large-scale, programmable deformation in response to external stimuli have great potential in many applications, including artificial muscles, robotics, and wearable devices. Despite their exciting prospects, limitations -such as few modes of shape transformation in a single actuator due to limited degree of freedom (DOF), difficulty to concurrently gain large length change and powerful stress, lack of scalable manufacturing method - seriously restrict their engineering applicability. Here we present bioinspired self-winding LCE fiber actuators that possess diverse controllable shape transformations (bending, twisting, coiling, and shortening), a combination of high contraction ratio (1750%) and high stress (~3.4 MPa), long term photomechanical robustness (over 1000 photodeformation cycles without obvious fatigue), and readily, scalable manufacture. Our fiber actuators can simultaneously conduct two or three kinds of deformation and thus enables complex morphing behaviors to manipulate objects (grabbing, dragging, lifting, and winding), and even drive gear set. We envision that these self-winding fiber actuators combined with high DOF, tunable actuation, photomechanical robustness, and mass production could be developed as high-performance artificial muscles for broad engineering applications.

1. Introduction

The development goal of man-made fiber actuators (artificial muscle) is to mimic structures and performances of human muscle which are organized in bundles of fibers and enable the generation of smooth motions and tunable strain/stress via controllable deformation of muscle fibers [1–3]. In the past decades, scientists have made considerable efforts to develop artificial muscles, and a broad range of soft active materials that resemble the deformation performance of human muscle has been reported such as responsive gels [4–7], shape memory polymers [8,9], conducting polymers [10,11], dielectric elastomers [12,13], liquid crystal elastomers (LCEs) [14–19]. Among them, LCEs that enable reversible, giant deformation (contraction up to 400−500%) [20] have been regarded as compelling soft active materials for artificial muscle, which was suggested by de Gennes as early as 1969 [21]. Since then, LCE fiber actuators (LCEFAs) have been prepared by various processing methods, including melt-drawing [22], microfluidic method [16], direct ink writing printing (DIWP) [23], and electrospinning [15]. Processing methods are responsible for not only just molding LCE materials into fiber shapes, but also inducing and regulating macroscopic liquid crystal (LC) orientation in the fiber, which is critically important to determine deformation and morphing behaviors of fabricated LCEFAs. However, the above-mentioned processing methods are only suitable for producing LCEFAs with uniform and simple LC director profiles in which LC mesogens are uniaxially aligned along the fibers' long axis without spatial difference of LC orientation. As a result, these uniaxial-oriented LCEFAs with uniform LC orientation usually only generate simple deformation of linear contraction or bending, exhibiting morphing behaviors with a low degree of freedom (DOF). Linear contraction arises from the uniform reduction of LC order of the uniaxial-oriented LCEFAs upon external stimuli (e.g. light, heating) [15,22], whereas bending deformation is generated through the formation of an uneven distribution of LC order over the fiber's cross-section, which is triggered by local or directional stimuli [24,25]. In recent years, to gain complex motions that require high DOF, twist insertion has been exploited to endow LCEFAs with

* Corresponding author at: Key Laboratory of 3D Micro/Nano Fabrication and Characterization of Zhejiang Province, School of Engineering, Westlake University, 18 Shilongshan Road, Hangzhou, Zhejiang Province 310024, China.
E-mail address: lvjiuan@westlake.edu.cn (J.-a. Lv).

https://doi.org/10.1016/j.apmt.2022.101449
2352-9407/

spiral LC director profiles, this asymmetrical alignment of LC enables rotating motion [26,27]. Despite these efforts, LCEFAs developed so far are still plagued with problems of few deformation modes and the inability to combine multiple deformations into a single actuator, due to their uniform and simple LC orientations. Moreover, large-scale manufacturing and difficulty concurrently gaining high length change and powerful stress represent great challenges in this area. Here, we show that those challenges can be tackled by a bioinspired screw-mold-based processing method. This versatile method not only possesses large-scale feasibility, but more importantly also enables inducing nonuniform and well-defined LC director profiles through a twistless strategy inspired by helix formation of plant-tendrils, which leads to diverse modes of deformation and tunable actuation achieved in the fabricated fiber actuators and thus enables high-DOF morphing behaviors.

High-DOF shape-changing materials are ubiquitous in the plant kingdom. Tendril is one of such materials that shows diverse high-DOF morphing behaviors (e.g. bending, twisting, coiling, and winding), when it changes shape from a linear structure into a helically coiled structure. The formation mechanism of the helix structure in plant tendrils can be explained by a simplified physical model of a filament with the bilayer structure. As shown in Fig. 1a, faster growth of top layer and slower growth of bottom layer result in internal strain/stress mismatch over the cross-section of the filament and leads to the intrinsic curvature that makes the filament self-winding to form a helical structure to avoid steric interactions when $L_0 > 2\pi R$ (Fig. 1b, L_0 denotes the filament' length; R indicates the radius of the arc of the curved filament) [28]. Here, it should be noted that the helix transformation in tendril is arising from the asymmetrical distribution of strain/stress over the plant's cross-section.

2. Results and discussion

Inspired by this biological mechanism, we created a processing method that enables facile, scalable, sustainable manufacture of self-winding LCE fiber actuators (SWLFAs) with high DOF and tunable actuations. We designed the method based on three criteria: (1) the fabricated fiber actuator must realize reversible shape transformation between a straight structure and a helix structure, thus providing high-DOF morphing behaviors; (2) length change and actuation stress must be tunable in a wide range in real-time; (3) the method must be easily conducted in materials lab and readily allow mass-production of fiber actuators. To meet the first requirement, asymmetrical distribution of strain/stress over the fiber's cross-section must be established. To that end, first, a screw-shaped mold was used to mold liquid crystal elastomer (LCE) oligomers into a helix-shaped precursor (soft spring) that has a length differential between its outer and inner circumference (Fig. 1d). Next, the soft spring precursor was straightened and stretched 50%, this stretching operation can induce the asymmetrical distribution of strain/stress over the cross-section of the stretched spring fiber (detail see Supplementary information). After maintaining the stretching for 24 h, the SWLFA with high-DOF was obtained (Fig. 1e). Unlike most previous reports that directly use the biological principle of plant tendril, relying on the precise design of the bilayers with mismatching strain to gain self-winding actuators, our approach makes use of a single phase with asymmetrical structure (soft spring precursor), thus avoiding delicate bilayer design [29–31]. To satisfy the second criteria, a photonic muscle made of a main-chain LCE mechanically enhanced by graphene was designed and used to prepare SWLFAs [20,32,33]. In contrast to sidechain LCEs, mainchain LCEs show the stronger chain anisotropy and allow for generating both strong force and large length change at the transition from the nematic to isotropic phase [34,35]. Moreover, graphene, which has excellent mechanical properties and photothermal effects [36], was selected as a functional dopant to enhance mechanical properties and endow the LCE with NIR response. The graphene owns a high Young's modulus up to 1 Tpa [37], and a small amount of doping can effectively improve Young's modulus of the soft LCE substrate and thus enhance the mechanical output of the composited LCE. In addition, graphene is a photothermal material with high thermal conductivity up to 5300 W m^{-1} K^{-1} [38], which can rapidly conduct thermal energy to trigger the doped LCE to change shapes. In addition, to gain large length change, we take advantage of the bioinspired helix transformation. During this transformation, SWLFAs make use of self-winding motion to transform from a long and straight structure to a stacked and compact coils structure, which can effectively amplify the length change [39]. Moreover, photoactive SWLFAs allow temporal and magnitude control of actuation strain/stress in real-time by modulation of light stimuli. The last requirement was satisfied by using simple screw molding and mechanical stretching to shape and align LCEs. Our method does not require delicate extrusion equipment, UV curing and temperature control equipment, the processing operation of the shaping LCEs by homemade screw molds plus following mechanical stretching at room temperature is enough to complete the fiber fabrication, which is convenient to be operated in any materials lab.

From these principles, we can mass-produce SWLFA with high DOF (Fig. 1f, SWLFA with a length of tens of meters can be readily prepared), which exhibits five distinct deformation behaviors (Fig. 1g): contracting, bending, twisting, coiling, and shortening. SWLFA's deformation behaviors can be remotely controlled by modulating incident NIR light beam. Bending deformation can be gained by point illumination using a thin NIR beam with a small diameter (2 mm), while contraction deformation can be induced by using a thick light beam with a diameter of 15 mm. Twisting, winding, and shortening deformations can also be controllably produced by a thick light beam but with different light intensities (Fig. S3c). Shortening deformation requires the strongest light intensity, winding deformation needs medium light intensity, and twisting deformation requires relatively lower light intensity (Fig. S3a). The response time of these deformations is on the scale of seconds depending on light intensity.

To figure out the actuation mechanisms of these five deformation modes, the shape-changing process of the SWLFA upon NIR irradiation was analyzed. Driven by liquid crystal phase transition and shape memory effect, the irradiated SWLFA can transform from a straight structure to a helix structure. During this helix transformation, the SWLFA exhibits three distinct stages of deformation (Fig. S6): *stage 1*, the SWLFA contracts and twists; *stage 2*, it bends and coils to form a coil spring; *stage 3*, the formed coil spring shortens the distance between the coils and turn to a compact spring. The light-induced shape-changing process of the SWLFA resembles the reverse of the morphing process of the soft spring precursor during the bioinspired stretching operation (Fig. S4). Contracting deformation is induced by light-induced reduction of LC order in the axial direction which leads the irradiated SWLFA to contraction along its long axis direction and expansion in the radial direction. Twisting arises from the light-trigged shape memory of the SWLFA that tends to return its twisted state (Fig. S7). Bending deformation is driven by the inherent curvature analogous to that of plant tendril. Owing to the presence of the gradient in order parameter over the cross-section of the SWLFA (Figs. S5 and S8a), the strain/stress difference between the inner side and the outer side of the SWLFA can be generated by light irradiation, which induces intrinsic curvature and leads to bending deformation (Fig. S8b). When the size (D) of the light beam is greater than $2\pi R'$ (R' denotes the radius of the arc of

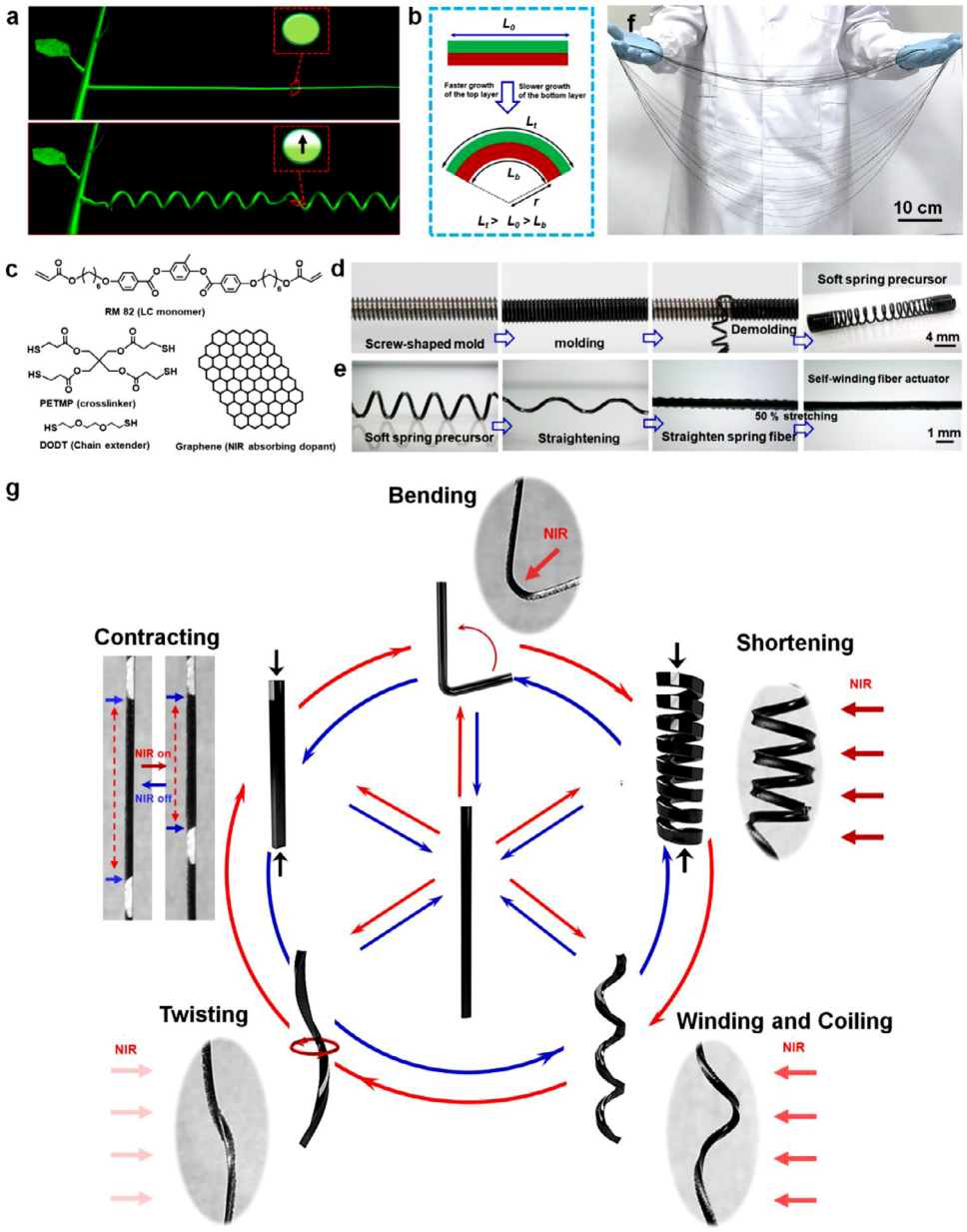

Fig. 1. Bioinspired design of self-winding fiber actuators. (a) Schematics showing a plant tendril transforming from a straight shape (top) into a helically coiled structure (bottom). The inset in the top photo shows that the cross-section of the straight tendril has a uniform distribution of strain/stress while the inset in the bottom image shows the coiled tendril possesses an asymmetrical distribution of strain/stress over its cross-section. (b) A simplified physic model with bilayer structure explains the generation of intrinsic curvature that leads to the shape transformation from a linear structure to the helix structure. (c) Chemical structures of the materials used for the preparation of the fiber actuators. (d) Experimental photographs showing how to use a screw mold to shape a liquid crystal elastomer (LCE) oligomer into the soft spring precursor. (e) Experimental photographs exhibiting the bioinspired stretching of soft spring precursor to prepare self-winding fiber actuator. (f) Photographs showing SWLFA with a length of tens of meters prepared in our lab. (g) Experimental photographs and corresponding schematics showing five different deformation behaviors in a self-winding fiber actuator. Black arrows show the contraction direction of the actuator. Red arrows indicate incident NIR light, and the shade of red arrows schematically indicates the intensity of the light (For interpretation of the references to color in this figure legend, the reader is referred to the web version of this article.).

bending SWLFA), the intrinsic curvature can induce self-coiling behavior to form a coil-spring structure to avoid steric interactions (Fig. S8). Furthermore, the continuous light radiation with sufficient intensity can trigger a strong shape memory effect to reduce the distance between the coils, generating shortening deformation (Fig. S5).

By regulating the size of the light spot as well as light intensity, we can effectively tune deformation modes and morphing behaviors of SWLFA. A small-sized light spot (D = 2 mm) illuminates the SWLFA, producing bending motion. The degree of bending can be well-defined by light intensity (Fig. S3b). Using a large light spot (D = 15 mm), we can regulate deformation modes of twisting, coiling/winding, and shortening by adjusting light intensity. When irradiated by the large spot with a relatively low intensity of 0.75 W cm^{-2}, the SWLFA only undergoes *stage 1* of deformation and displays contracting and twisting behaviors featured in this stage. When the light intensity is increased to 1.0 W cm^{-2}, the SWLFA can undergo *stage 1* and *stage 2*, producing more deformation modes (contracting, twisting, and coiling). As the light intensity further increases to 2.0 W cm^{-2}, the SWLFA can undergo all three stages, exhibiting all the five deformation modes (contracting, twisting, coiling, bending, and shortening). The light in-

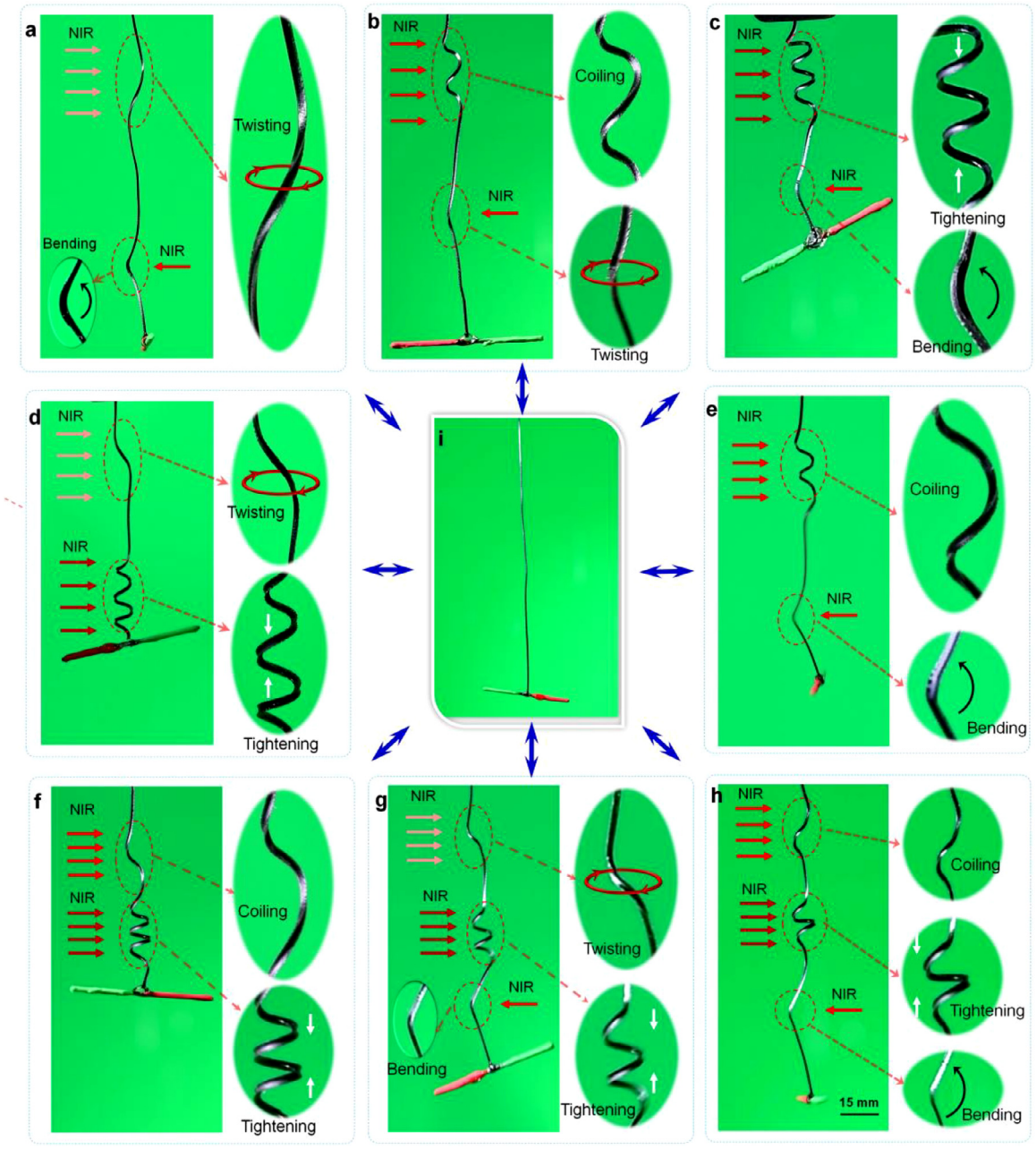

Fig. 2. Experimental photographs showing SWLFA simultaneous generation of multiply deformations. (a) Combination of twisting and bending. (b) Combination of coiling and twisting. (c) Combination of tightening and bending. (d) Combination of twisting and tightening. (e) Combination of coiling and bending. (f) Combination of coiling and tightening. (g) Combination of twisting, tightening, and bending. (h) Combination of coiling, tightening, and bending. (i) image shows the initial shape of SWLFA. Red arrows indicate incident NIR light. The shades of red arrows denote the intensity of used NIR light. A long rod was hung at the end of the SWLFA to help clearly show light-induced deformation behaviors of the SWLFA (For interpretation of the references to color in this figure legend, the reader is referred to the web version of this article.).

tensity determines how many stages of deformation the SWLFA can go through, so it can be leveraged to regulate deformation modes. It is worth noting that the diversity of deformation modes shown by SWLFAs is also related to the weight of the load. The heavy load can suppress the SWLFAs to generate high-DOF motions (e.g. coiling, winding), decreasing the diversity of deformation modes. Furthermore, when multiple light sources with tunable intensities and spot sizes are used to illuminate different parts of one SWLFA, complex deformations that combine controllable multiple modes can be achieved simultaneously in the single fiber actuator.

We demonstrate that SWLFA possesses the capability to simultaneously exert different deformation modes. As shown in Fig. 2, two or even three deformation modes can be simultaneously achieved in one SWLFA. As a result, various compound operations that combine bending, rotation, and lifting can be realized. This high-DOF actuation feature is of great significance for robotic arm and micromechanical systems [40]. In nature, tentacles of the octopus, biological soft actuators - possess remarkable morphing capabilities that both allow to respectively generate diverse deformation behavior at any part along their length, such as twisting, changing length, bending, and winding, and enable simultaneous producing two or more deformation behaviors at desired parts along one tentacle [41,42]. However, simultaneous generation of various controllable deformations in a synthetic soft actuator has been proved challenging, whereas as demonstrated in Fig. 3,

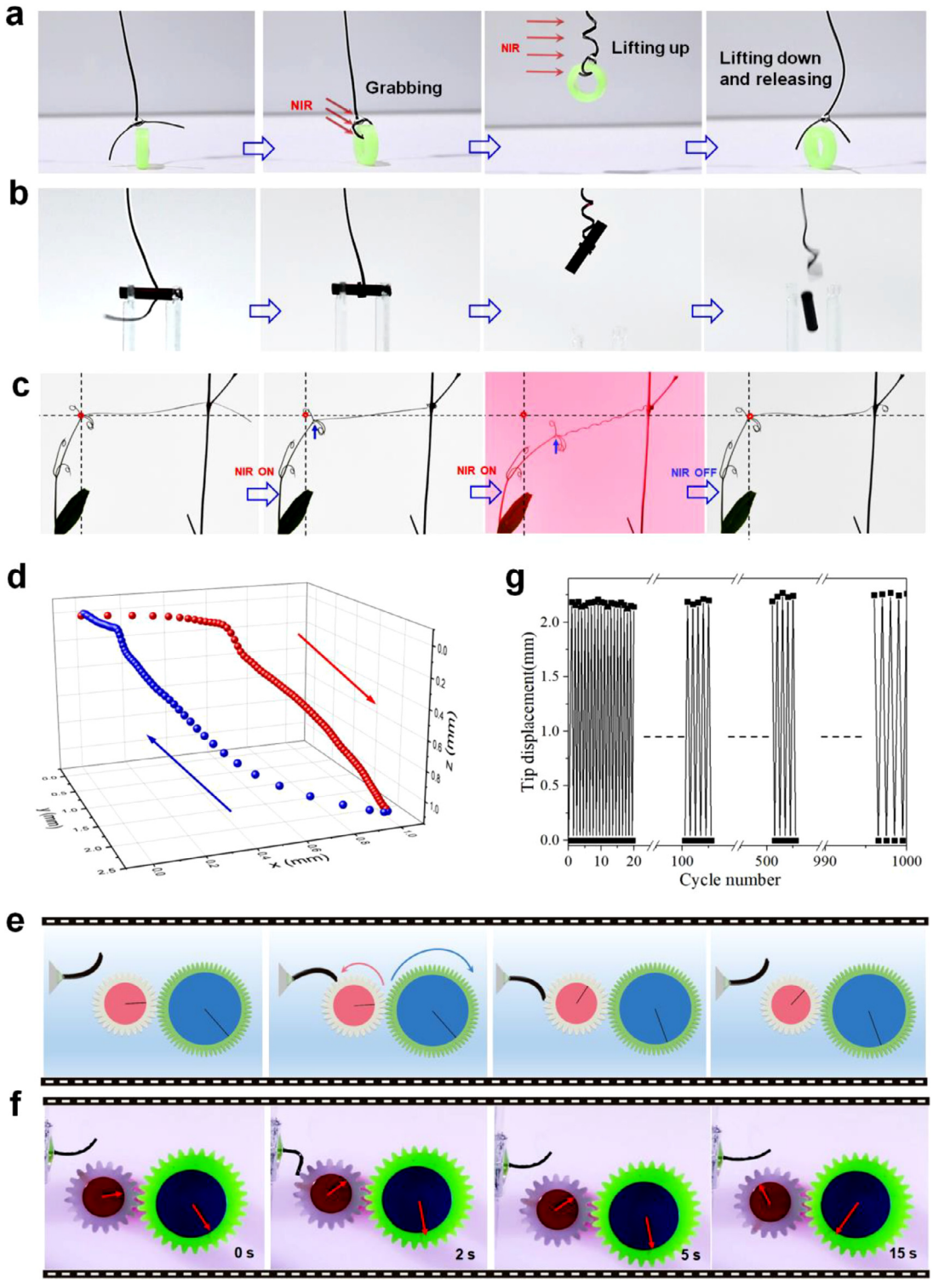

Fig. 3. Functionalities arising from high-DOF deformation of SWLFA. (a) Snapshots showing photomanipulation of SWLFA-made soft arm to grip, drag, lift up, lift down, and then release a ring-shaped object with the weight of 58 mg (Supplementary Movie 1). (b) Snapshots showing SWLFA self-winding to grasp a rod-shaped object, lifting upwards, and finally releasing it (Supplementary Movie 2). (c) Snapshots showing photocontrol of SWLFA mimicking the biological behavior of tendril (Supplementary Movie 3). The SWLFA first employs the winding motion to attach to the plant stem, then it self-coils to shorten and pull itself close to the stem. (d) Diagram showing 3D loop-shaped moving trajectory of the free end of SWLFA under one cycle of on-and-off illumination. (e,f) schematics (top) and experimental photographs (bottom) showing photocontrol of SWLFA to generate non-planar bending to drive gearwheel rotation (Supplementary Movie 4). (g) 1000 cycles of non-planar bending of SWLFA without obvious fatigue.

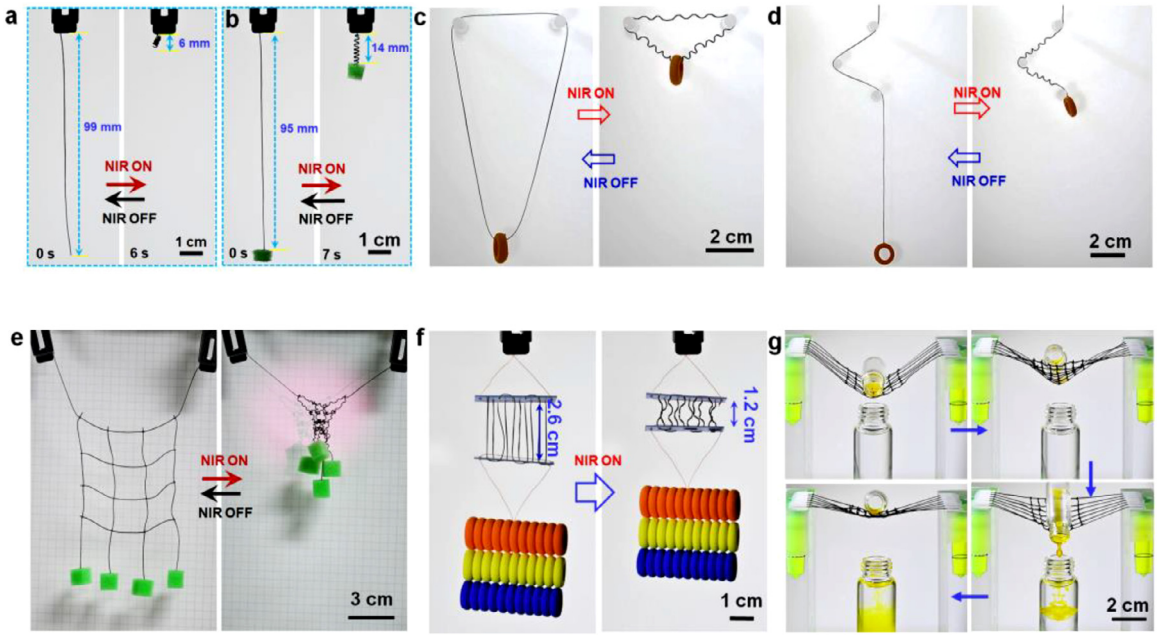

Fig. 4. Versatile Functionalities arising from the unique combination of powerful actuation stress with large length change. (a) Photographs showing SWLFA fast, reversible light-driven shape transformation between a linear structure and a helix structure with large length change (Supplementary Movie 5). The intensity of 808 nm light is 2.0 W cm^{-2}, and the length of the straight fiber actuator is 99 mm. (b) Photographs showing SWLFA loaded with a heavy object exhibiting fast reversible helix transformation (Supplementary Movie 6). The intensity of 808 nm light is 2.0 W cm^{-2}, the length of the straight fiber actuator is 95 mm. The mass of the fiber and the load are 5.6 mg and 5.1 mg, respectively. (c) A loop-shaped microlifter translating winding into vertical lifting (Supplementary Movie 7). The length of the fiber actuator is 32.3 cm. The mass of fiber and load is 19.4 mg and 52 mg, respectively. (d) SWLFA can curve along splines to lift a load (Supplementary Movie 8). The intensity of 808 nm light is 2.5 W cm^{-2}, the length of the fiber is 18.8 cm. The mass of the fiber and the load is 11.3 mg and 52 mg, respectively. (e) Photographs showing the area change of a mesh-shaped actuator woven by SWLFAs (Supplementary Movie 10). Upon light illumination, this actuator can change its area from 36 cm^2 to 3.3 cm^2, and the area change is up to 1090%. The size of the mesh is 6 cm × 6 cm, and the net hole size is 2 cm × 2 cm. The intensity of 808 nm light is 3 W cm^{-2}. (f) Multiple SWLFAs are used to enhance light-induced force (Supplementary Movie 9). The intensity of 808 nm light is 3.5 W cm^{-2}. The mass of the load is 2 g. (g) Photographs showing the mesh-shaped actuator loaded a container with yellow-colored liquid were manipulated to lift and tilt the container, and then pour out the yellow liquid into a targeted vial (Supplementary Movie 11). The intensity of 808 nm light is 3 W cm^{-2}. The size of the mesh is 3 cm × 3 cm, and the net hole size is 5 mm × 5 mm. The mass of the vial is 2.8 g (For interpretation of the references to color in this figure legend, the reader is referred to the web version of this article.).

SWLFA shows a similar capability that simultaneously and locally generates multiple deformation behaviors. This ability to combine various deformations in a single soft actuator endow SWLFAs with flexibility and adaptability to handle a complex array of movements, which can significantly broaden functionalities and application horizons [43]. As shown in Fig. 3a, taking advantage of high DOFs-deformation, SWLFA can not only achieve grasping, rotating, lifting up and down, and releasing a ring-shaped object (Supplementary Movie 1), but also enable winding, grabbing, and lifting a cylinder-shaped object - a direct mimicry of grasping function of octopus' tentacles (Fig. 3b, Supplementary Movie 2). Moreover, we demonstrate that SWLFA can behave like a plant tendril and employ programmable shape-morphing to wind around and tether to an adjacent plant stem, and then employ helix transformation to shorten its distance to the stem (Fig. 3c, Supplementary Movie 3). These biological behaviors allow tendril lifting for advantageous ecological niches (rich sunshine and space, etc.) as well as offer enhanced reliability against external environmental impacts (strong wind, heavy rain, etc.) [29].

Small-scale, mechanical operations are of great significance for advanced industrial and technological applications. Taking advantage of powerful actuation and asymmetrical deformation behaviors (Fig. 3d), SWLFA can be used to directly transduce light energy into mechanical work to drive gearwheel rotation (Fig. 3e and f, Supplementary Movie 4), exhibiting an effective and feasible approach to continuously covert light energy to mechanical power, which is vital for engineering applications in microsystems, such as microelectromechanical systems (MEMS) and Lab on a chip. In addition, SWLFA allows continuous photomechanical work lasting more than 1000 deformation cycles without obvious fatigue (Fig. 3g), demonstrating high reliability that is critically important for real engineering applications.

As shown in Fig. 4a, SWLFA exhibits fast, reversible light-driven shape transformation between a linear structure and a helix structure with large length change (Supplementary Movie 5). When in the case of loading a heavy object that is close to its weight, SWLFA can also gain the fast reversible helix transformation (Fig. 4b, Supplementary Movie 6). Moreover, the soft nature of SWLFA enables it to adapt to complex environments, the loop-shaped SWLFA can convert length contraction into lifting in the vertical direction Fig. 4.d and e show that SWLFA can curve along splines to lift a load (Supplementary Movie 7,8). As shown in Fig. 4f, we can increase light-induced excitation force by integrating multiple SWLFAs (Supplementary Movie 9). As shown in Fig. 4g, we weaved SWLFA into a mesh-shaped actuator. Upon light illumination, this actuator can vary its area from 36 to 3.3 cm^2, and the area change is up to 1090% (Supplementary Movie 10). Finally, we demonstrate that the mesh-shaped actuator loaded a container with yellow-colored liquid was manipulated to lift and tilt a container, and then pour out the yellow liquid into a targeted vial (Fig. 4h, Supplementary Movie 11), exhibiting multi-DOF behaviors crucial for micromechanical operation and engineering.

As shown in Fig. 5, SWLFA exhibits a combination of large length change and corresponding high stress. SWLFA shows a contraction ratio up to 1750% with a fast actuation rate of 258% s^{-1} when the light intensity reaches 3 W cm^{-2} (Figs. 5a and S10). According to our knowledge, the highest record of the contraction ratio of LCEs is ~500% (Fig. 5e). Here, it should note that the length change of SWLFA, like other soft actuators, is inversely

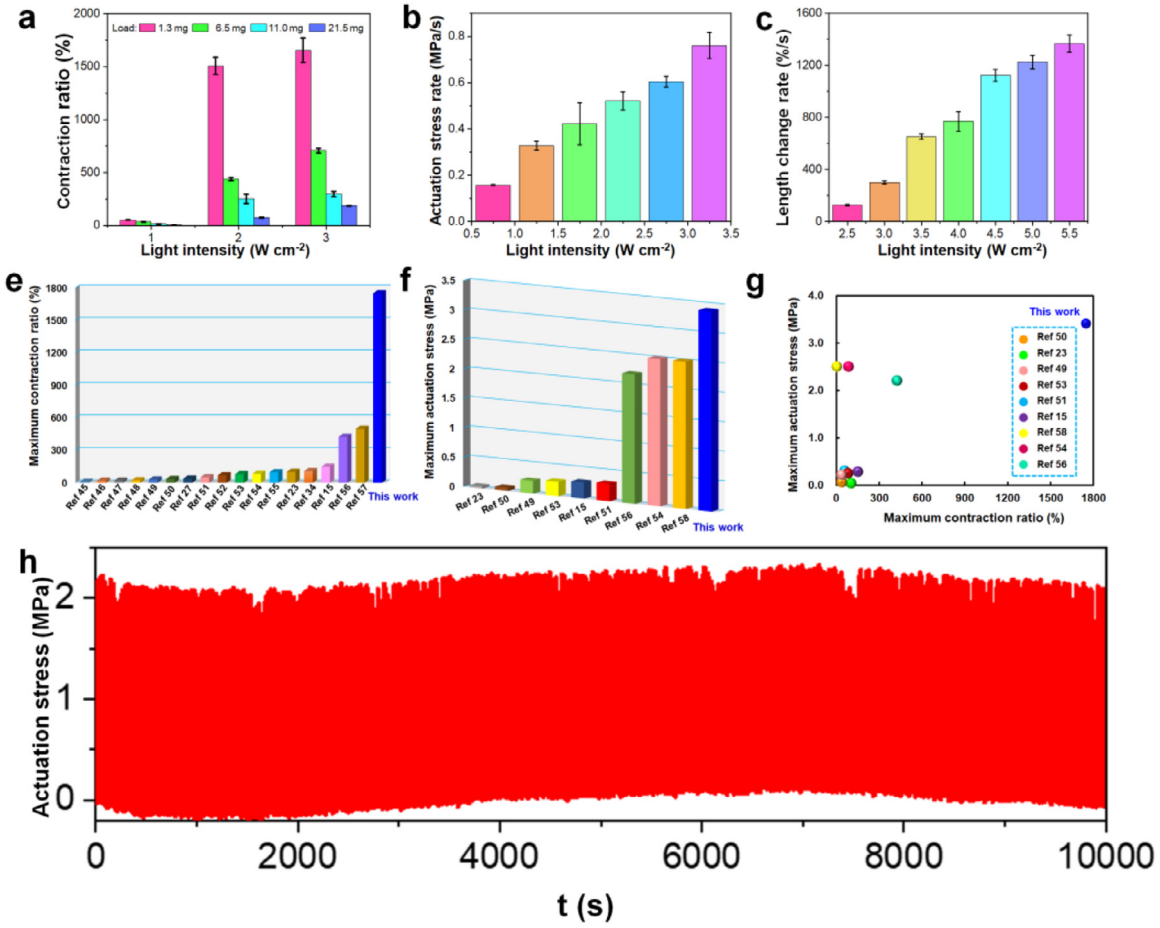

Fig. 5. Comparative actuation-performance charts for LCP-based fiber actuators. (a) plots exhibiting that the contraction ratio of SWLFA is proportional to light intensity and inversely proportional to the weight of the load. (b,c) plots showing the rate of actuation stress and length change is proportional to light intensity, respectively. (e,f) comparative summary of maximum contraction ratio and length change in previous representative reports and this work, respectively [45–58]. (g) Comparative stress/length-change charts for PLCP-based actuators [49–51,53,54,56,58] (h) 1000 following cycles of generating the stress of ~2 MPa.

proportional to loaded weight [29,44]. Nevertheless, SWLFA can still gain a remarkable contraction ratio of 150% when bearing a heavy load that is 13 times heavier than the weight of the SWLFA (Figs. 5a and S10). In addition, SWLFA also demonstrates a powerful actuation force. As shown in Fig. 5b, it can generate powerful light-induced stress up to 3.4 MPa with a rapid actuation rate of 0.34 MPa s^{-1} (Fig. S11). The previously reported maximum record of light-induced stress of LCE-based actuators is ~2.5 MPa (Fig. 5f). These actuation characteristics place SWLFA in a previously inaccessible region of stress-strain charts of LCE-based fiber actuators (Fig. 5g). Moreover, SWLFA undergoes 1000 continuous deformation cycles to repeat generation of strong stress of ~2 MPa without obvious fatigue (Fig. 5h), demonstrating its high reliability crucial for practical applications.

3. Conclusion

In this report, we designed and prepared a triple high-DOF, high-stress, high-length-change fiber actuator. The high-DOF feature of SWLFA not only enables controllable generation of various deformations (contracting, twisting, bending, coiling, and shortening), but also conducts composite behaviors that simultaneously combine diverse deformations, even mimic complex biological deformation behaviors in living organisms. With the integration of the spring-like structure transformation, we can optimize both actuation stress and length change at once. Moreover, the manufacture of SWLFAs does not need access to expensive facilities or complex processing operations, which enables any materials lab to employ our fabrication method to mass-produce SWLFAs. With mass production of SWLFAs with tunable mechanics and photodeformation, we are currently exploring SWLFA as the structural unit to assemble and build hierarchical, complex soft actuators via advanced assembly technologies (e.g. programmable weaving). It is anticipated that the development of our manufacturing approach of SWFLAs would enable mass production of artificial muscle that meets engineering requirements in actuation performance, mechanical robustness, manufacturability, reliability and cost-effectiveness.

Declaration of Competing Interest

The authors declare that they have no known competing interest.

CRediT authorship contribution statement

Zhiming Hu: Conceptualization, Methodology, Formal analysis, Investigation, Validation, Writing – original draft, Writing – review & editing. **Yunlong Li:** Methodology, Validation, Formal analysis, Investigation, Writing – review & editing. **Tonghui Zhao:** Methodology, Validation, Formal analysis, Investigation, Writing – review & editing. **Jiu-an Lv:** Conceptualization, Funding acquisition, Formal analysis, Investigation, Project administration, Supervision, Writing – review & editing.

Acknowledgments

This research was supported by National Natural Science Foundation of China (51873197), Natural Science Foundation of Zhejiang Province of China (LR22E030004), 151 Talent Project of Zhejiang Province, and Foundation of Westlake University.

Supplementary materials

Supplementary material associated with this article can be found, in the online version, at doi:10.1016/j.apmt.2022.101449.

References

[1] J. Xiong, J. Chen, P.S. Lee, Functional fibers and fabrics for soft robotics, wearables, and human–robot interface, Adv. Mater. 33 (2021) e2002640, doi:10.1002/adma.202002640.
[2] C. Gotti, A. Sensini, A. Zucchelli, R. Carloni, M.L. Focarete, Hierarchical fibrous structures for muscle-inspired soft-actuators: a review, Appl. Mater. Today 20 (2020) 100772, doi:10.1016/j.apmt.2020.100772.
[3] Y. Wang, C. Liu, L. Ren, L. Ren, Bioinspired soft actuators with highly ordered skeletal muscle structures, Biodes. Manuf. (2021), doi:10.1007/s42242-021-00148-1.
[4] X. Qian, Y. Zhao, Y. Alsaid, X. Wang, M. Hua, T. Galy, H. Gopalakrishna, Y. Yang, J. Cui, N. Liu, M. Marszewski, L. Pilon, H. Jiang, X. He, Artificial phototropism for omnidirectional tracking and harvesting of light, Nat. Nanotechnol. 14 (2019) 1048, doi:10.1038/s41565-019-0562-3.
[5] M. Zhou, J. Gong, J. Ma, Continuous fabrication of near-infrared light responsive bilayer hydrogel fibers based on microfluidic spinning, e-Polymers 19 (2019) 215–224, doi:10.1515/epoly-2019-0022.
[6] S.H. Kim, J.H. Jeong, H. Shim, H.C. Woo, K.B.C. Imani, J. Yoon, J.H. Jeong, M.H. Kim, Water-responsive tough 1D hydrogel with programmable deformations for actuators and chemical sensors, Smart Mater. Struct. 30 (2021) 075014, doi:10.1088/1361-665X/ac028d.
[7] P. Lv, X. Yang, H.K. Bisoyi, H. Zeng, X. Zhang, Y. Chen, P. Xue, S. Shi, A. Priimagi, L. Wang, W. Feng, Li Q, Stimulus-driven liquid metal and liquid crystal network actuators for programmable soft robotics, Angew. Chem. Int. Ed. 60 (2021) 3390, doi:10.1039/D1MH00623A.
[8] Q. Shen, S. Trabia, T. Stalbaum, V. Palmre, K. Kim, I.K. Oh, A multiple-shape memory polymermetal composite actuator capable of programmable control, creating complex 3D motion of bending, twisting, and oscillation, Sci. Rep. 6 (2016) 24462, doi:10.1038/srep24462.
[9] X. Qi, W. Yang, L. Yu, W. Wang, H. Lu, Y. Wu, S. Zhu, Y. Zhu, X. Liu, Y. Dong, Y. Fu, Design of ethylene-vinyl acetate copolymer fiber with two-way shape memory effect, Polymers 11 (2019) 1599 (Basel), doi:10.3390/polym11101599.
[10] S.V. Ebadi, H. Fashandi, D. Semnani, B. Rezaei, A. Fakhrali, Electroactive actuator based on polyurethane nanofibers coated with polypyrrole through electrochemical polymerization: a competent method for developing artificial muscles, Smart Mater. Struct. 29 (2020) 045008, doi:10.1088/1361-665X/ab73e5.
[11] T.L. Buckner, R.A. Bilodeau, S.Y. Kim, R. Kramer-Bottiglio, Roboticizing fabric by integrating functional fibers, Proc. Natl. Acad. Sci. U.S.A. 117 (2020) 25360, doi:10.1073/pnas.2006211117.
[12] L. Liu, C. Zhang, M. Luo, X. Chen, D. Li, H. Chen, A biologically inspired artificial muscle based on fiber-reinforced and electropneumatic dielectric elastomers, Smart Mater. Struct. 26 (2017) 085018, doi:10.1088/1361-665X/aa723f.
[13] M. Duduta, E. Hajiesmaili, H. Zhao, R.J. Wood, D.R. Clarke, Realizing the potential of dielectric elastomer artificial muscles, Proc. Natl. Acad. Sci. U.S.A. 116 (2019) 2476, doi:10.1073/pnas.1815053116.
[14] X. Lin, M.O. Saed, E.M. Terentjev, Continuous spinning aligned liquid crystal elastomer fibers with a 3D printer setup, Soft Matter 17 (2021) 5436, doi:10.1039/D1SM00432H.
[15] Q. He, Z. Wang, Y. Wang, Z. Wang, C. Li, R. Annapooranan, J. Zeng, R. Chen, S. Cai, Electrospun liquid crystal elastomer microfiber actuator, Sci. Robot. 6 (2021) eabi9704, doi:10.1126/scirobotics.abi9704.
[16] E.K. Fleischmann, F.R. Forst, R. Zentel, Liquid-crystalline elastomer fibers prepared in a microfluidic device, Macromol. Chem. Phys. 215 (2014) 1004, doi:10.1002/macp.201400008.
[17] J. Ma, Y. Yang, C. Valenzuela, X. Zhang, L. Wang, W. Feng, Mechanochromic, shape-programmable and self-healable cholesteric liquid crystal elastomers enabled by dynamic covalent boronic ester bonds, Angew. Chem. Int. Ed. (2022) e202116219, doi:10.1002/anie.202116219.
[18] J. Yang, X. Zhang, X. Zhang, L. Wang, W. Feng, Q. Li, Beyond the visible: bioinspired Infrared adaptive materials, Adv. Mater. 33 (2021) 2004754, doi:10.1002/adma.202004754.
[19] P. Lv, X. Yang, H.K. Bisoyi, H. Zeng, X. Zhang, Y. Chen, P. Xue, S. Shi, A. Priimagi, L. Wang, W. Feng, Q. Li, Stimulus-driven liquid metal and liquid crystal network actuators for programmable soft robotics, Mater. Horiz. 8 (2021) 2475, doi:10.1039/D1MH00623A.
[20] H. Yang, A. Buguin, J.M. Taulemesse, K. Kaneko, S. Meŕy, A. Bergeret, P. Keller, Micron-sized main-chain liquid crystalline elastomer actuators with ultralarge amplitude contractions, J. Am. Chem. Soc. 131 (2009) 15000, doi:10.1016/0375-9601(69)90584-2.
[21] P.G. de Gennes, Possibilites offertes par lareticulation de polymeres presence d'un cristal liquide, Phys. Lett. 28A (1969) 725, doi:10.1021/ja905363f.
[22] J. Naciri, A. Srinivasan, H. Jeon, N. Nikolov, P. Keller, B.R. Ratna, Nematic elastomer fiber actuator, Macromolecules 36 (2003) 8499, doi:10.1021/ma034921g.
[23] D.J. Roach, C. Yuan, X. Kuang, V.C. Li, P. Blake, M.L. Romero, I. Hammel, K. Yu, H.J. Qi, Long liquid crystal elastomer fibers with large reversible actuation strains for smart textiles and artificial muscles, ACS Appl. Mater. Interfaces 11 (2019) 19514, doi:10.1021/acsami.9b04401.
[24] T. Yoshino, M. Kondo, J. Mamiya, M. Kinoshita, Y. Yu, T. Ikeda, Three-dimensional photomobility of crosslinked azobenzene liquid-crystalline polymer fibers, Adv. Mater. 22 (2010) 1361, doi:10.1002/adma.200902879.
[25] Y. Yu, L. Li, E. Liu, X. Han, J. Wang, Y. Xie, C. Lu, Light-driven core-shell fiber actuator based on carbon nanotubes/liquid crystal elastomer for artificial muscle and phototropic locomotion, Carbon 187 (2022) 97 N Y, doi:10.1016/j.carbon.2021.10.071.
[26] Y. Wang, J. Sun, W. Liao, Z. Yang, Liquid crystal elastomer twist fibers toward rotating microengines, Adv. Mater. (2022) 2107840, doi:10.1002/adma.202107840.
[27] S. Nocentini, D. Martella, D.S. Wiersma, C. Parmeggiani, Beam steering by liquid crystal elastomer fibres, Soft Matter 13 (2017) 8590, doi:10.1039/C7SM02063E.
[28] T. McMillen, A. Goriely, Tendril perversion in intrinsically curved rods, J. Nonlinear Sci. 12 (2002) 241, doi:10.1007/s00332-002-0493-1.
[29] Y. Cheng, R. Wang, K.H. Chan, X. Lu, J. Sun, G.W. Ho, A biomimetic conductive tendril for ultrastretchable and integratable electronics, muscles, and sensors, ACS Nano 12 (2018) 3898, doi:10.1021/acsnano.8b01372.
[30] J. Liu, J. Huang, T. Su, K. Bertoldi, D.R. Clarke, Structural transition from helices to hemihelices, PLoS ONE 9 (2014) e93183, doi:10.1371/journal.pone.0139525.
[31] Y. Chen, J. Yang, X. Zhang, Y. Feng, H. Zeng, L. Wang, Feng W, Light-driven bimorph soft actuators: design, fabrication, and properties, Mater. Horiz. 8 (2021) 728, doi:10.1039/D0MH01406K.
[32] J. Yuan, W. Neri, C. Zakri, P. Merzeau, K. Kratz, A. Lendlein, P. Poulin, Shape memory nanocomposite fibers for untethered high-energy microengines, Science 365 (2019) 155, doi:10.1126/science.aaw3722.
[33] J. Foroughi, G. Spinks, Carbon nanotube and graphene fiber artificial muscles, Nanoscale Adv. 1 (2019) 4592, doi:10.1039/C9NA00038K.
[34] L. Liu, M.H. Liu, L.L. Deng, B.P. Lin, H. Yang, Near-infrared chromophore functionalized soft actuator with ultrafast photoresponsive speed and superior mechanical property, J. Am. Chem. Soc. 139 (2017) 11333, doi:10.1021/jacs.7b06410.
[35] C. Ohm, M. Brehmer, R. Zentel, Liquid crystalline elastomers as actuators and sensors, Adv. Mater. 22 (2010) 3366, doi:10.1002/adma.200904059.
[36] Z. Li, H. Lei, A. Kan, H. Xie, W. Yu, Photothermal applications based on graphene and its derivatives: a state-of-the-art review, Energy 216 (2021) 119262, doi:10.1016/j.energy.2020.119262.
[37] C. Lee, X. Wei, J.W. Kysar, J. Hone, Measurement of the elastic properties and intrinsic strength of monolayer graphene, Science 321 (2008) 385, doi:10.1126/science.1157996.
[38] A.A. Balandin, S. Ghosh, W. Bao, I. Calizo, D. Teweldebrhan, F. Miao, C.N. Lau, Superior thermal conductivity of single-layer graphene, Nano Lett. 8 (2008) 902, doi:10.1021/nl0731872.
[39] M. Kanik, S. Orguc3, G. Varnavides, J. Kim, T. Benavides, D. Gonzalez, T. Akintilo, C.C. Tasan, A.P. Chandrakasan, Y. Fink, P. Anikeeva, Strain-programmable fiber-based artificial muscle, Science 365 (2019) 145–150, doi:10.1126/science.aaw2502.
[40] T.J. Wallin, J. Pikul, R.F. Shepherd, 3D printing of soft robotic systems, Nat. Rev. Mater. 3 (2018) 84, doi:10.1038/s41578-018-0002-2.
[41] C. Laschi, M. Cianchetti, B. Mazzolai, L. Margheri, M. Follador, P. Dario, Soft robot arm inspired by the octopus, Adv. Robot. 26 (2012) 709, doi:10.1163/156855312x626343.
[42] S. Min, J. Won, S. Lee, J. Park, J. Lee, Softcon: simulation and control of soft-bodied animals with biomimetic actuators, ACM Trans. Graph. 38 (2019) 1, doi:10.1145/3355089.3356497.
[43] I.D. Walker, D.M. Dawson, T. Flash, F.W. Grasso, R.T. Hanlon, B. Hochner, W.M. Kier, C.C. Pagano, C.D. Rahn, Q.M. Zhang, Continuum robot arms inspired by cephalopods, Proc. SPIE. Unmanned Ground Vehicle Technology VII, 5804 (2005) 303, doi:10.1117/12.606201.
[44] X. Wang, S.K. Mitchell, E.H. Rumley, P. Rothemund, C. Keplinger, High-strain peano-HASEL actuators, Adv. Funct. Mater. 30 (2019) 1908821, doi:10.1002/adfm.201908821.
[45] K.M. Lee, T.J. Bunning, T.J. White, Autonomous, hands-free shape memory in glassy, liquid crystalline polymer networks, Adv. Mater. 24 (2012) 2839, doi:10.1002/adma.201200374.
[46] M.H. Li, P. Keller, J. Yang, P.A. Albouy, An artificial muscle with lamellar structure based on a nematic triblock copolymer, Adv. Mater. 16 (2004) 1922, doi:10.1002/adma.200400658.
[47] M.H. Li, P. Keller, B. Li, X. Wang, M. Brunet, Light-driven side-on nematic elastomer actuations, Adv. Mater. 15 (2003) 569, doi:10.1002/adma.200304552.
[48] H. Finkelmann, E. Nishikawa, G.G. Pereira, M. Warner, A new opto-mechanical effect in solids, Phys. Rev. Lett. 87 (2001) 015501, doi:10.1103/PhysRevLett.87.015501.
[49] E.H. Cho, K. Luu, S.Y. Park, Mechano-actuated light-responsive main-chain liquid crystal elastomers, Macromolecules 54 (2021) 5397, doi:10.1021/acs.macromol.1c00088.

[50] M. Wang, Y. Song, H.K. Bisoyi, J.F. Yang, L. Liu, H. Yang, Q. Li, A liquid crystal elastomer-based unprecedented two-way shape-memory aerogel, Adv. Sci. 8 (2021) e2102674, doi:10.1002/advs.202102674.
[51] P.T. Elliott, L. Xing, W.H. Wetzel, J.E. Glass, Influence of terminal hydrophobe branching on the aqueous solution behavior of model hydrophobically modified ethoxylated urethane associative thickeners, Macromolecules 36 (2003) 8449, doi:10.1021/ma020166f.
[52] H. Yang, M.X. Liu, Y.W. Yao, P.Y. Tao, B.P. Lin, P. Keller, X.Q. Zhang, Y. Sun, L.X. Guo, Polysiloxane-based liquid crystalline polymers and elastomers prepared by thiol−ene chemistry, Macromolecules 46 (2013) 3406, doi:10.1021/ma400462e.
[53] D.L. Thomsen, P. Keller, J. Naciri, R. Pink, H. Jeon, D. Shenoy, B.R. Ratna, Liquid crystal elastomers with mechanical properties of a muscle, Macromolecules 34 (2001) 5868, doi:10.1021/ma001639q.
[54] H.F. Lu, M. Wang, X.M. Chen, B.P. Lin, H. Yang, Interpenetrating liquid-crystal polyurethane/polyacrylate elastomer with ultrastrong mechanical property, J. Am. Chem. Soc. 141 (2019) 14364, doi:10.1021/jacs.9b06757.
[55] L. Yu, H. Shahsavan, G. Rivers, C. Zhang, P. Si, B. Zhao, Programmable 3D shape changes in liquid crystal polymer networks of uniaxial orientation, Adv. Funct. Mater. 28 (2018) 1802809, doi:10.1002/adfm.201802809.
[56] X. Pang, L. Qin, B. Xu, Q. Liu, Y. Yu, Ultralarge contraction directed by light-driven unlocking of prestored strain energy in linear liquid crystal polymer fibers, Adv. Funct. Mater. 30 (2020) 2002451, doi:10.1002/adfm.202002451.
[57] S.V. Ahir, A.R. Tajbakhsh, E.M. Terentjev, Self-assembled shape-memory fibers of triblock liquid-crystal polymers, Adv. Funct. Mater. 16 (2006) 556, doi:10.1002/adfm.200500692.
[58] M. Kondo, M. Sugimoto, M. Yamada, Y. Naka, J. Mamiya, M. Kinoshita, A. Shishido, Y. Yu, T. Ikeda, Effect of concentration of photoactive chromophores on photomechanical properties of crosslinked azobenzene liquid-crystalline polymers, J. Mater. Chem. 20 (2010) 117, doi:10.1039/B917342K.